Biointerface Research in Applied Chemistry
Open-Access Journal (ISSN: 2069-5837)

Article
Volume 15, Issue 5, 2025, 67
https://doi.org/10.33263/BRIAC155.067

In Silico Evaluation of Cellulose, Chitosan, and Metal Clusters (Cu_{18} and Au_{32}) for Ethylene Control Material in Postharvest Agriculture

Art Anthony Z. Munio [1,*], Charmie B. Munio [2], Renzo Miguel R. Hisona [3], Alvanh Alem G. Pido [4], Leo Cristobal C. Ambolode II [5,6]

1 Department of Physics, Western Mindanao State University, 7000 Zamboanga City, Philippines
2 Agricultural and Biosystems Engineering Department, Jose Rizal Memorial State University, 7116 Tampilisan, Philippines
3 College of Fisheries and Aquatic Sciences, North Eastern Mindanao State University – Lianga Campus, 8307 Lianga, Philippines
4 Department of Physics, Mindanao State University-Main Campus, 9700 Marawi City, Philippines
5 Department of Physics, Mindanao State University–Iligan Institute of Technology, 9200 Iligan City, Philippines
6 Center for Nanoscience Research, Premier Research Institute of Science and Mathematics (PRISM), Mindanao State University–Iligan Institute of Technology, 9200 Iligan City, Philippines
* Correspondence: munio.art@wmsu.edu.ph;

Received: 20.05.2025; Accepted: 22.07.2025; Published: 10.08.2025

Effective ethylene (C_2H_4) control technology in postharvest agriculture is critical for minimizing crop wastage and improving supply chain efficiency. Here, we simulate the adsorption of C_2H_4 on cellulose, chitosan, copper cluster, and gold cluster using the framework of density functional theory. In all studied complexes, the adsorption processes of C_2H_4 are spontaneous, indicated by negative adsorption energies. The interaction of C_2H_4 with cellulose and chitosan is generally described as physisorption, where minimal orbital hybridization is visible and long-range interaction distances are measured. The low magnitude of adsorption energies yields a recovery time of 10^{-11}-10^{-9} s at 298 K under UV incident radiation. The results of both copper and gold clusters show that the magnitude of adsorption can be in the regime of chemisorption and physisorption. In addition, the recovery time for copper and gold clusters can reach the range of 10^2 s and 10^1 s, respectively. The electron localization function and frontier orbitals revealed a strong hybridization between the copper and gold clusters with C_2H_4, further explaining the claim. The chemisorption character is also evident in the increased absorption intensities in the UV region of copper and gold clusters upon C_2H_4 adsorption. These observations are potential sensing properties of the metal cluster for ethylene. The analysis of the electronic density of states revealed that the copper and gold clusters generally maintain their metallicity after the attachment of the C_2H_4, except for minor broadening of peaks. The paper provides an in-depth perspective on C_2H_4 adsorption with biopolymers and metal clusters, providing future insights and clarifying previous experimental studies. These findings will serve as a reference for designing selective and low-cost materials for C_2H_4 regulation technologies in postharvest agriculture.

Keywords: ethylene; cellulose; chitosan; metal cluster; copper cluster; gold cluster; adsorption; density functional theory; adsorbent; sensor; postharvest agriculture; ethylene control; ethylene adsorbent.

1. Introduction

Ethylene (C_2H_4) control technologies for postharvest storage for climacteric fruits and vegetables are crucial as they can minimize crop wastage during the postharvest stage [1,2]. Surveys indicate that wastage of fruits and vegetables can range from 20% to 50% in the supply chain [3,4]. One of the prominent problems is the uncontrolled ripening of climacteric fruits and vegetables. Less than 1.0 ppm of C_2H_4 in storing climacteric fruits and vegetables will trigger the biochemical activity related to respiration [5]. It is, therefore, relevant to develop technologies that can trap and detect C_2H_4 molecules to improve postharvest management. Various C_2H_4 regulators are currently utilized in the market. Standard C_2H_4 control technologies used natural zeolites, titanium dioxide (TiO_2), activated carbon, potassium permanganate ($KMnO_4$), and C_2H_4 inhibitors [3,6,7]. However, few efforts have been made to maximize the potential of cellulose, chitosan, and metal clusters for C_2H_4 control.

The importance of biopolymers has found its way into many applications, ranging from building materials, adsorbents, filters, and even electronics [8]. In particular, the interest in biopolymers stems from their associated eco-friendly properties, low cost, scalability, and compatibility with high-performance nanomaterials. Aligned with this are the transition metal nanoparticles widely investigated in various application technologies, including chemical adsorbents and sensor technologies [9–13]. For example, cellulose modified with a cationic polyelectrolyte polyvinyl amine polymer filter effectively removes bacteria [14]. The composite of chitosan, graphene oxide, and ZnO was successfully fabricated and tested to capture CO_2 with only a 4.35% loss of adsorption performance after ten cycles [15]. Similarly, metal clusters are also established materials in many applications. For instance, it is revealed that gold nanoparticles (AuNP) are effective as a colorimetric sensor for detecting cations, anions, and small molecules such as glucose, dopamine, and cysteine [16]. In other work, copper-based nanoparticles can function as and be selective for CO_2 gas separation, antimicrobial, and dye adsorbents [17,18]. Despite the diverse reports on applying cellulose, chitosan, copper-based, and metal nanoparticles for sorbent technologies, foundational studies on C_2H_4 adsorbed on these materials are scarce. Detailed research evaluating the C_2H_4 adsorption on various materials will be crucial for discovering effective adsorbents and sensor technology to mitigate wastage in fresh produce.

The experimentation on the performance of materials for adsorbent applications is costly and relies heavily on trial-and-error procedures. To reduce the cost and time, quantum-based simulations are used to study the behavior of electrons in a crystal or molecular structures; this is useful for predicting exotic properties of new materials, providing proof-of-concept for materials application, and explaining experimental findings [19–22]. For example, the evaluation of graphene oxide using the DFT framework shows that it can help trap perfluorinated compounds in water systems [23]. Other work revealed that the interaction of gas molecules adsorbed on MXenes demonstrates their sensing performance and explains the underlying concepts [24–26]. Although the simulation of the C_2H_4 interface with various materials is generally limited, we have found few studies studying TiO_2, doped-graphene, and metal clusters in complexes with C_2H_4 [27–31]. Most research interest, however, lies in the mechanism of catalysis rather than in the adsorbent and sensor function.

In this work, we explain the adsorption mechanism of the C_2H_4 molecule on the surface of cellulose, chitosan, Cu_{18} cluster, and Au_{32} cluster using the density functional theory with dispersion correction. The findings reveal that the adsorptions are all exothermic reactions.

Strong adsorption is computed with the Cu_{18}-C_2H_4 and Au_{32}-C_2H_4 complexes. In contrast, the low magnitude of the adsorption energy and long-range interaction distances are measured for the cellulose-C_2H_4 and chitosan-C_2H_4 complexes. The density of states and UV-Vis spectra reveal a potential sensing performance of the Au cluster. Overall, this work demonstrates the proof-of-concept of biopolymers and metal clusters as trapping material for C_2H_4 and explains the mechanism behind the adsorption. With these findings, we anticipate this work will help narrow down the potential materials for C_2H_4 control technologies.

2. Computational Details

All simulations are performed using the Quantum ESPRESSO code for materials modeling [32,33]. The optimized norm-conserving pseudopotentials and the Perdew-Burke-Ernzerhof (PBE) functionals are used to treat the exchange-correlation contributions of the studied systems [34,35]. The plane-wave energy and charge cutoffs are set to 60 Ry and 240 Ry, respectively. For the self-consistent field (SCF) calculation, an energy tolerance of 10^{-8} Ry is used for the convergence with Gaussian smearing to speed up the convergence. The treatment of dispersion between intermolecular systems is described by the Grimme-D3 correction, which shows good agreement with experimental values with minimal increase in the simulation time [36]. At least a 15 Å vacuum is introduced between adjacent images to minimize the interaction between isolated structures. The Broyden–Fletcher–Goldfarb–Shanno (BFGS) algorithm is used to optimize the calculations of the atomic structures. The optimized atomic configuration of the systems is estimated using the standard force and energy convergence tolerance of 10^{-4} Ry/Bohr and 10^{-4} Ry, respectively. The gamma-point algorithm is used in all optimization computations.

The affinity of the C_2H_4 on the cellulose and chitosan is quantified by the adsorption energy E_{Ad}, which is defined as

$$E_{Ad} = E_{Complex} - E_{Adsorbent} - E_{Ethylene} \quad (1)$$

Here, $E_{Complex}$, $E_{Adsorbent}$, and $E_{Ethylene}$ denote the total energy of the complex, as well as the adsorbent material and C_2H_4. The recovery time, T_R of the C_2H_4 on the adsorption sites, is computed using the following formula,

$$T_R = \frac{1}{\upsilon_o} e^{-\frac{E_{Ad}}{k_B T}} \quad (2)$$

The Boltzmann constant, temperature, and incident radiation frequency are denoted by k_B, T, and υ_o, respectively. The T_R is the duration for an adsorbent to release the attached C_2H_4, allowing the materials to return to their original state.

To characterize the bonding character of the studied complexes, we compute the electron localization function (ELF). The ELF provides a measure of the likelihood of finding an electron pair in a given region of space defined as follows [37],

$$ELF = \frac{1}{1+\chi(r)} \quad \text{where} \quad \chi(r) = \frac{\frac{1}{2}\sum_{i=1}^{N}|\nabla\psi_i|^2 - \frac{1}{8}\frac{\nabla n(r)}{n(r)}}{\frac{3}{10}(3\pi^2)^{\frac{3}{2}} n(r)^{\frac{5}{3}}} \quad (3)$$

Here, $n(\mathbf{r})$ and ψ depict the electron density and wavefunctions, respectively. The ELF has been proven helpful in distinguishing the nature of bonds within molecules and materials. The value of the ELF ranges from zero to unity, where ELF > 0.7 indicates electron localization similar to a chemical bond, and 0.2 < ELF < 0.7 indicates metallic bonding characteristics. The atomic configurations, ELF 2D contour, and frontier orbitals isosurface are plotted using VESTA [38,39].

To compute the electronic density of states of the Cu_{18}-C_2H_4 and Au_{32}-C_2H_4 complexes, we used the hybrid PBE0 functional to treat bandgap underestimation of the PBE. The absorbance intensity of the Cu_{18}-C_2H_4 and Au_{32}-C_2H_4 complexes is estimated using time-dependent density functional theory (TDDFT), applying the Liouville-Lanczos approach [40,41]. A total of 3,000 Lanczos iterations is used to calculate the spectrum as benchmarked from the reference [40].

3. Results and Discussion

First, the ground-state atomic configurations of cellulose and chitosan biopolymers are analyzed and validated with available experimental data. Next, the complex's adsorption energy, recovery time, interaction distance, and bandgap are examined to quantify the bonding characteristics. The electron localization function (ELF) and isosurface of frontier molecular orbitals are discussed to visualize the hybridization of electrons and their topology. These analyses are repeated for the discussion on Cu_{18}-C_2H_4 and Au_{32}-C_2H_4 complexes with additional information on the density of states and UV-Vis absorption spectra.

The cellulose and chitosan molecular models are modeled with four units comprising 87 atoms and 91 atoms, respectively. We compare these optimized structures with experimental results to validate the molecular models and the level of theory used. In the optimized configuration, the measured units of cellulose and chitosan are 10.51 Å and 10.24 Å, respectively. Meanwhile, experiments show that the dimensions of the unit of cellulose and chitosan in crystal form are 10.38 Å and 10.31 Å, respectively [42,43]. We highlight that the main difference is that the prototype structure is isolated with only two units, while experiments are in a bulk structure and at a higher degree of polymerization. Nevertheless, the disagreement for the unit length for cellulose and chitosan is only 1.25% and 0.67%, respectively. Furthermore, the measured bandgap of cellulose and chitosan is 4.45 eV and 4.02 eV, while experimental reports give 4.5 eV and 4.07 eV [44,45]. This comparison demonstrates DFT's predictive capability to estimate and confirm experimental values, even at the PBE level treatment of the exchange-correlation functional.

Now, we analyze C_2H_4 adsorption on the cellulose and chitosan using equation (1). According to Table 1, the calculated adsorption energy of C_2H_4 on the cellulose ranges from -0.16 eV to -0.20 eV, and chitosan has values ranging from -0.09 eV to -0.21 eV. All configurations of the cellulose-C_2H_4 (Figure 1) and chitosan-C_2H_4 (Figure 2) complexes maintain an interaction distance of 2.42 Å to 2.75 Å. For both cellulose-C_2H_4 and chitosan-C_2H_4 complexes, it is observed that the strong interactions of C_2H_4 attached to the backbone of cellulose and chitosan, mainly due to wider surface interactions, as depicted in Figure 1(c) and (d) and Figure 2(c) and (d). Compared with literature, the E_{Ads} values' magnitude is lower than that of the $B_{12}P_{12}$ cluster, with adsorbed C_2H_4 having an energy of -0.32 eV (-30.7 kJ/mol) [46]. These computed E_{Ads} are also close to the graphene-C_2H_4 and WSe_2-C_2H_4 systems with adsorption energies of -0.14 eV and -0.19 eV, respectively [31]. From an experimental perspective, a notable work by Rad et al. shows that the chitosan-rich films show poor bonding

performance of C_2H_4 compared to zeolite-rich films [47]. These findings support our claim that C_2H_4 weakly interacts with the chitosan.

Table 1. List of the adsorption energy (eV), recovery time (s), equilibrium interaction distance (Å), and bandgap (eV) of C_2H_4 adsorption on various sites of cellulose, chitosan, Cu_{18}, and Au_{32}. The estimated bandgap at the GGA-PBE level approximation for cellulose, chitosan, Cu_{18}, and Au_{32} is 4.45 eV, 4.02 eV, 0.67 eV, and 1.54 eV, respectively.

Systems	Adsorption energy (eV) E_{Ad}	Recovery time (s) T_R	Interaction distance (Å) d_{min}	Bandgap (eV) E_{gap}	Bonding description
Cellulose - C_2H_4					
Configuration – 1	-0.16	5×10^{-10}	2.42	4.32	Physisorption
Configuration – 2	-0.16	5×10^{-10}	2.44	4.35	Physisorption
Configuration – 3	-0.20	3×10^{-9}	2.62	4.31	Physisorption
Configuration – 4	-0.20	2×10^{-9}	2.75	4.30	Physisorption
Chitosan - C_2H_4					
Configuration – 1	-0.09	3×10^{-11}	2.64	4.06	Physisorption
Configuration – 2	-0.09	3×10^{-11}	2.60	4.03	Physisorption
Configuration – 3	-0.21	3×10^{-9}	2.65	4.02	Physisorption
Configuration – 4	-0.21	3×10^{-9}	2.72	3.98	Physisorption
Cu_{18} - C_2H_4					
Configuration – 1	-0.85	3×10^{2}	2.12	0.51	Chemisorption
Configuration – 2	-0.18	1×10^{-9}	2.69	0.69	Physisorption
Configuration – 3	-0.82	8×10^{1}	2.12	0.68	Chemisorption
Au_{32} - C_2H_4					
Configuration – 1	-0.75	4×10^{0}	2.27	1.40	Chemisorption
Configuration – 2	-0.32	2×10^{-10}	4.28	1.53	Physisorption
Configuration – 3	-0.74	4×10^{0}	2.28	1.40	Chemisorption

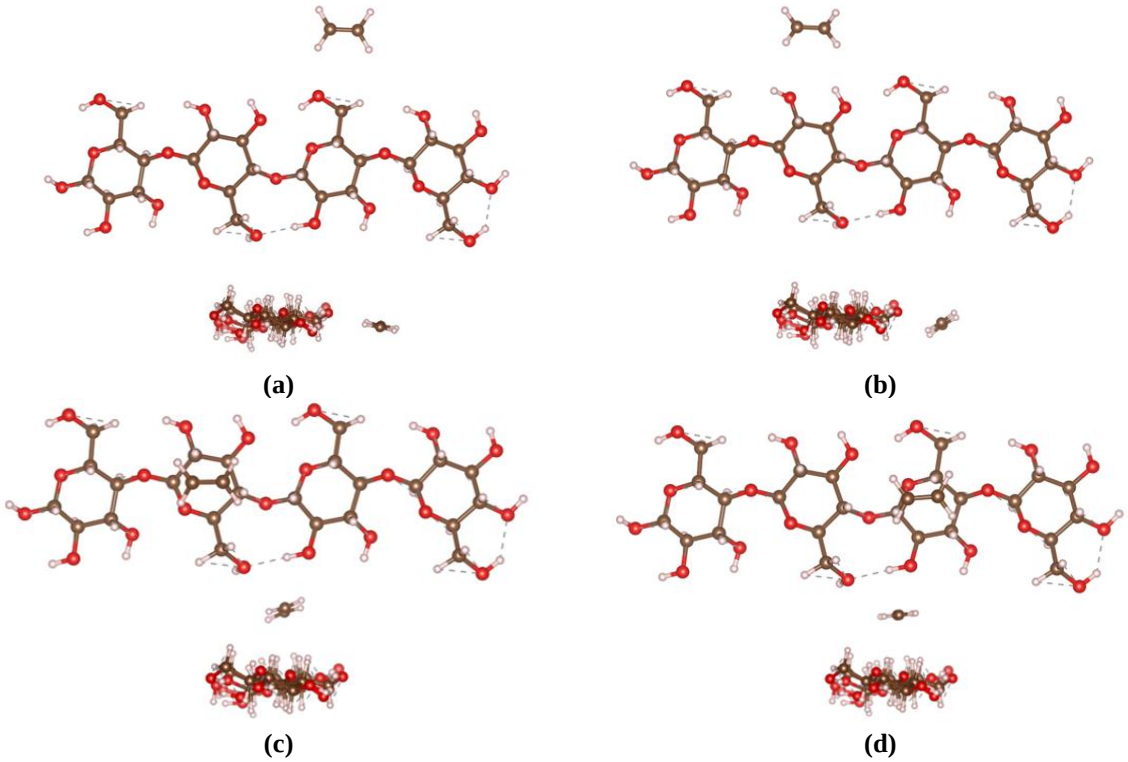

Figure 1. Optimized molecular configurations of C_2H_4 adsorbed on cellulose: **(a)** Configuration-1 (near the hydroxymethyl group); **(b)** Configuration-2 (near the hydroxyl group); **(c)** Configuration-3 (on the cellulose backbone); **(d)** Configuration-4 (on the cellulose backbone).

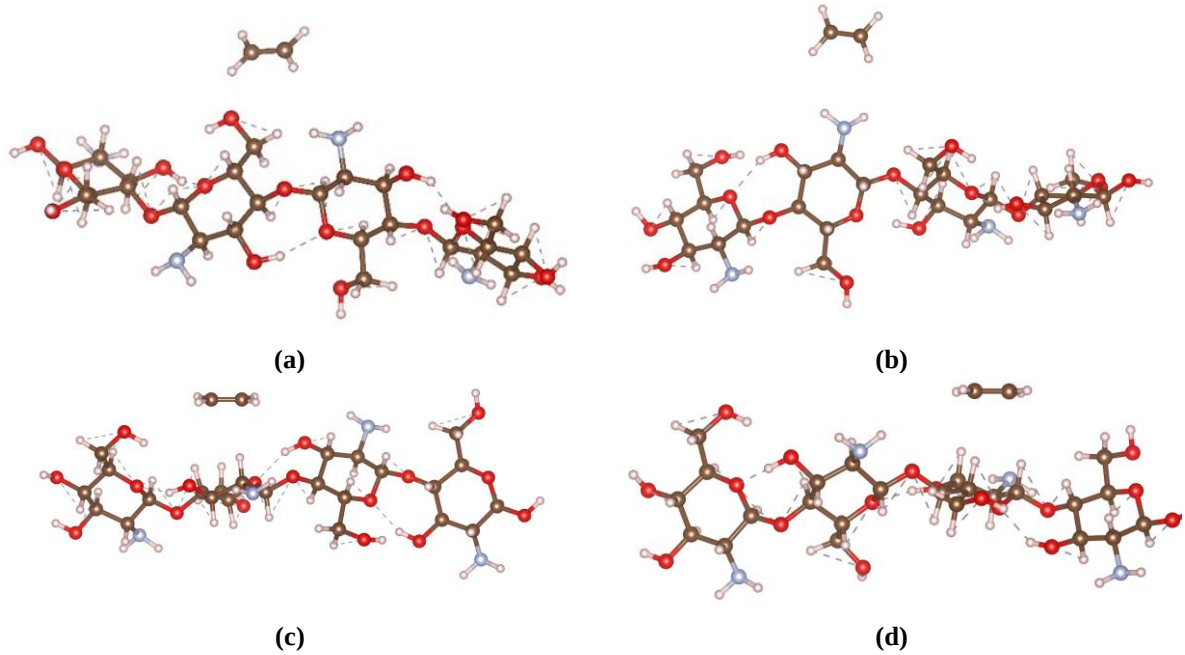

Figure 2. Optimized molecular configurations of C_2H_4 adsorbed on the cellulose: **(a)** Configuration-1 (near the hydroxymethyl group); **(b)** Configuration-2 (near the amine group); **(c)** Configuration-3 (on the chitosan backbone); **(d)** Configuration-4 (on the chitosan backbone).

To quantify the estimated time for the C_2H_4 to be released from the adsorption site under the influence of UV radiation at 298 K, the recovery time is computed using equation (2). Table 1 lists the recovery time (T_R) for C_2H_4 in cellulose and chitosan as 0.5-3 ns and 0.03-3 ns, respectively. The interaction is maximized when C_2H_4 is adsorbed on the cellulose and chitosan backbone. This result is a characteristic of physisorption, where a wider interface area leads to stronger adsorption energy. The short T_R is due to the weak adsorption energy and long-range interaction distances. It is suggested that the C_2H_4 molecule can easily desorb on the surface of cellulose and chitosan.

Turning to the Cu_{18} and Au_{32} clusters with adsorbed C_2H_4, both systems yield a maximum magnitude of adsorption energy of -0.85 eV (Figure 3a) and -0.75 eV (Figure 4a), respectively. Weaker E_{Ads} are computed in Figure 3(b) and Figure 4(b), where both complexes yield longer interaction distances of 2.69 Å and 4.28 Å. The results in Figure 3(c) and Figure 4(c) reproduce the trend in the adsorption energy of Orientation-1 of both complexes, revealing multiple strong binding sites for C_2H_4 adsorption. In comparison, for a Cu(110)-C_2H_4, results range from -0.076 eV to -0.60 eV using B3LYP hybrid functional [48]. Other reports on Au cluster-C_2H_4 yield a magnitude of 0.53 eV to 1.58 eV in a π mode interaction, i.e., when two C atoms of C_2H_4 bind with a single Au atom of the cluster [49].

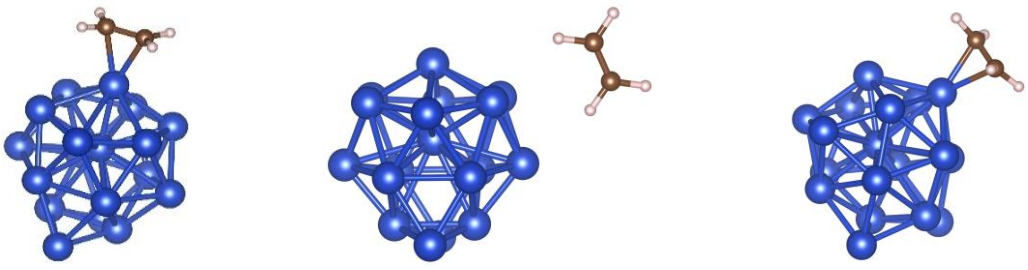

Figure 3. Optimized molecular configuration of Cu_{18}-C_2H_4 complexes: **(a)** Orientation-1; **(b)** Orientation-2; **(c)** Orientation-3.

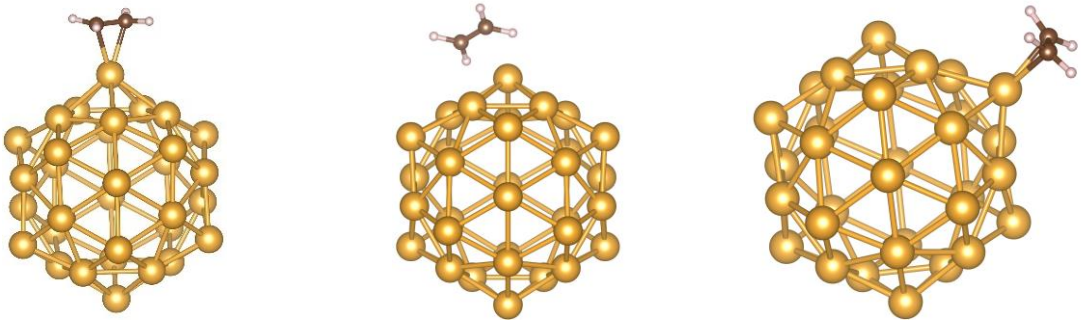

(a) **(b)** **(c)**

Figure 4. Optimized molecular configuration of Au_{32}-C_2H_4 complexes: **(a)** Orientation-1; **(b)** Orientation-2; **(c)** Orientation-3.

To improve our understanding at the fundamental level, we plot the frontier molecular orbitals of the optimized molecular structures. Figures 5(a) and (b) display the highest and lowest molecular orbitals of cellulose and chitosan with the C_2H_4 molecule represented by an isosurface set at 5 $\times 10^{-4}$ e/Å^2. In both cases, minimal hybridization of the orbital characters is visible, which is the usual nature of weakly bonded systems. This characteristic is also noticed in systems where the adsorption energies' magnitude is lower than 0.5 eV. In reference to the ELF definition provided in equation (3), the ELF 2D contour plot revealed that blue basins represent low values of ELF. This confirms that the primary interaction is mainly due to minor charge redistributions, which drive the attractive electrostatic interaction.

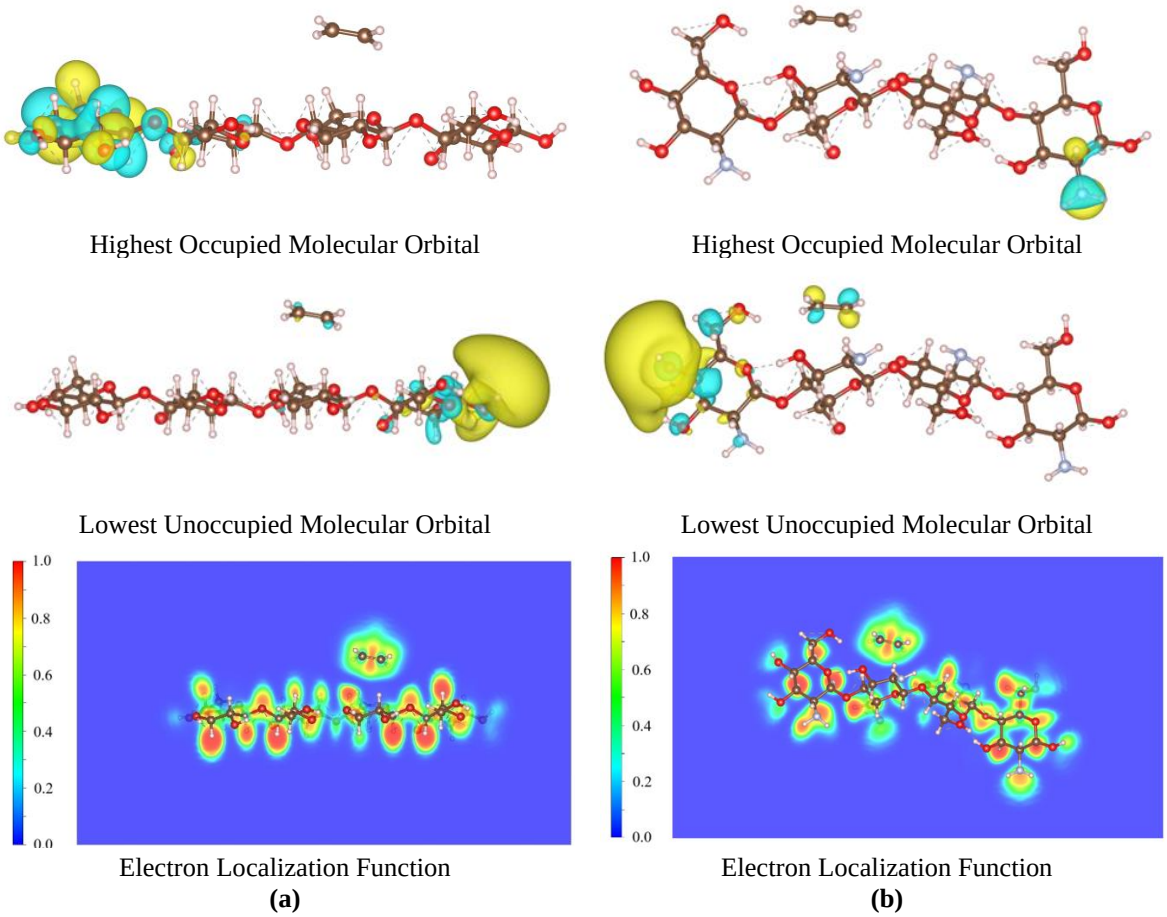

(a) **(b)**

Figure 5. Highest occupied molecular orbital (HOMO), lowest unoccupied molecular orbital (LUMO), and electron localization function (ELF) of **(a)** cellulose-C_2H_4; **(b)** chitosan-C_2H_4 complexes. The isosurface of the molecular orbital is set to 0.0005 e/Å^2.

Turning our attention to metal clusters, Figures 6(a) and (b) show the frontier orbital distribution of Cu_{18}-C_2H_4 and Au_{32}-C_2H_4 complexes, respectively. The Cu_{18}-C_2H_4 highest occupied molecular orbital (HOMO) overlapped, indicating strong hybridization of orbitals between constituents. This type of hybridization was not observed in cellulose-C_2H_4 and chitosan complexes, clearly distinguishing their nature of bonding. Meanwhile, for Au_{32}-C_2H_4, it is observed that the lowest unoccupied molecular orbital (LUMO) is hybridized. Both of these findings demonstrate the strong bonding between constituents. These results are also verified by the 2D ELF contour of the complexes presented in Figures 6(a) and (b). The ELF basins of Cu_{18} and C_2H_4 overlapped, and the cyan basin at the interface indicates a metallic bonding, indicated by the value of the ELF of 0.2-0.3. Such results are also noted in the Au_{32}-C_2H_4 complex, in which the ELF of the constituents overlaps. Overall, these electron topologies display that Cu_{18} and Au_{32} are good trapping materials for C_2H_4 because the shared electron type of bonding results in strong adsorption energy.

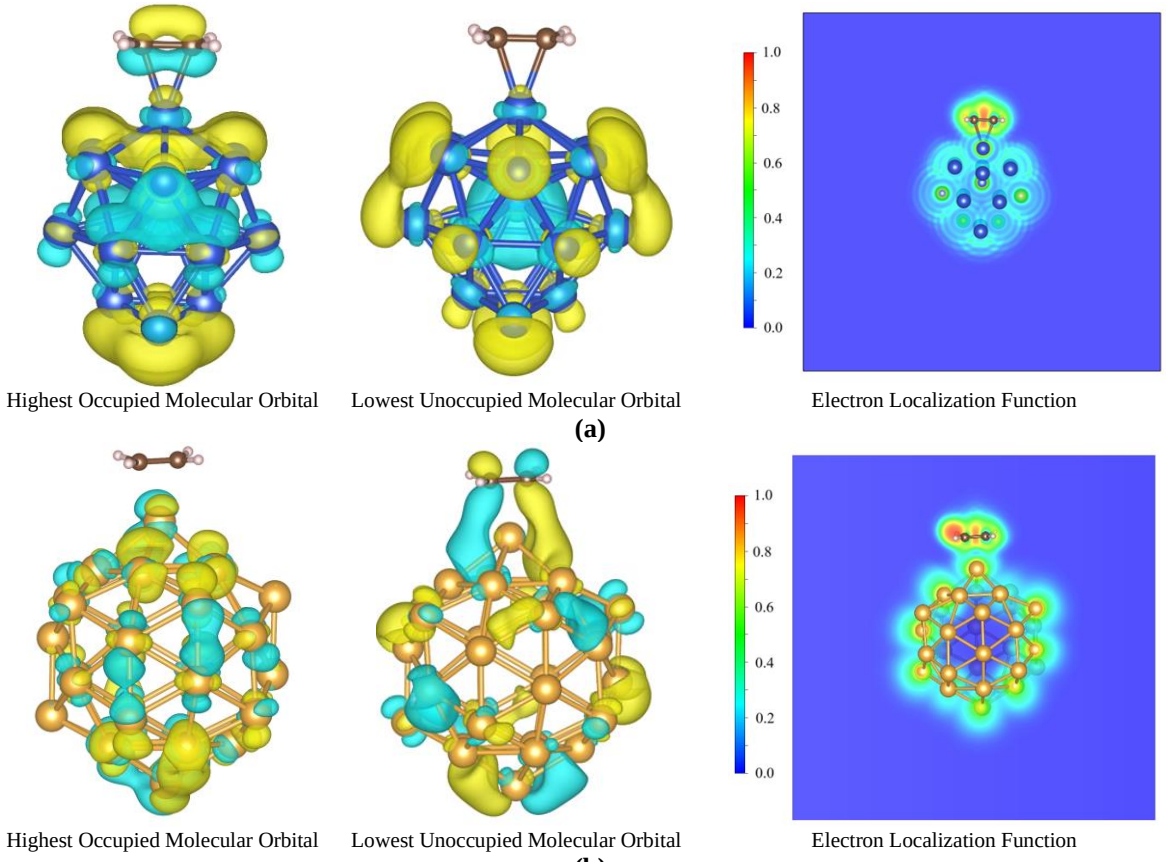

Figure 6. Highest occupied molecular orbital (HOMO), lowest unoccupied molecular orbital (LUMO), and electron localization function (ELF) of (a) Cu_{18}-C_2H_4; (b) Au_{32}-C_2H_4 complexes. The isosurface of the molecular orbital is set to 0.0005 e/Å2.

Due to the strong interaction of the metal clusters and C_2H_4, the density of states of the Cu_{18}-C_2H_4 and Au_{32}-C_2H_4 complexes are computed and presented in Figures 7(a) and (b), respectively. The density of states is crucial for understanding the bonding characteristics and providing insights into the electrical and optical properties. It is evident in Figure 7a that the density of states of Cu_{18} and minor alignment of the states are visible upon adsorption of C_2H_4. Orientation-1 of the Cu_{18}-C_2H_4 complex yields a significant decrease in the bandgap to 0.51 eV from 0.67 eV measured for isolated Cu_{18}. Meanwhile, Orientation-2 and Orientation-3 of the Cu_{18}-C_2H_4 complexes give a bandgap of 0.69 eV and 0.68 eV, respectively. For Au_{32}-C_2H_4

complexes, it is computed that the Au_{32}-C_2H_4 complex gives 1.40 eV (Configuration – 1), 1.53 eV (Configuration – 2), and 1.40 eV (Configuration-3). Such a bandgap value is close to the isolated bandgap of Au_{32} (1.54 eV).

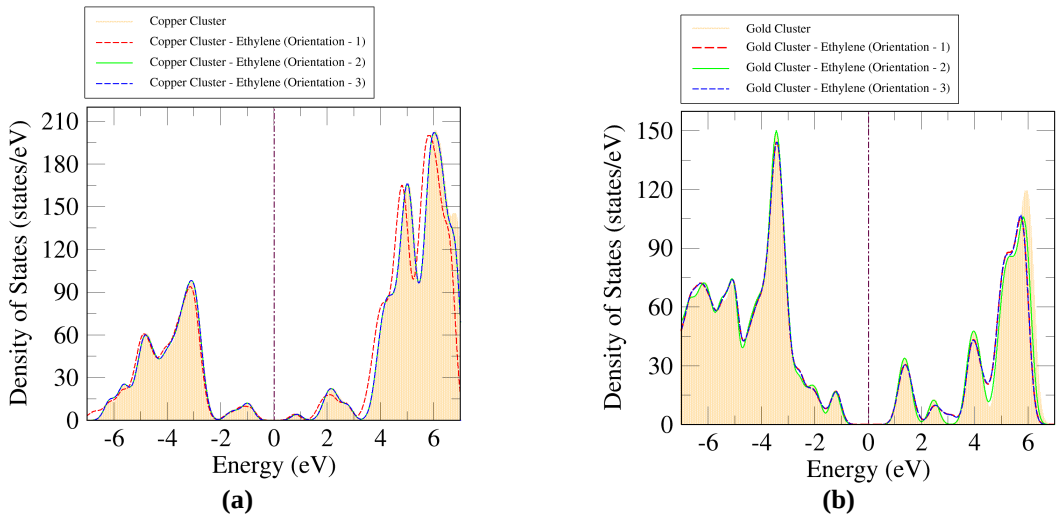

Figure 7. Total electronic density of states of **(a)** Cu_{18}-C_2H_4; **(b)** Au_{32}-C_2H_4 complexes in various bonding orientations. The Fermi energy is set to 0 eV, represented by the vertical maroon dashed line.

In general, the sensitivity of the material's bandgap in response to attached analyte can be utilized as a sensing criterion. The sensing ability can be quantified by measuring the sensing material's electrical or optical properties [50]. Here, we simulate the UV-Vis spectra of Cu_{18} and Au_{32} with attached C_2H_4 using time-dependent density functional theory to give an additional perspective on the observables. Figure 8 shows that the adsorption of C_2H_4 on the Cu_{18} and Au_{32} increases the absorption intensity in the UV region. For the Cu_{18} cluster, the initial peak at 213 nm shifted to 227 nm, 217 nm, and 217 nm for Orientation-1, Orientation-2, and Orientation-3, respectively. For the Au_{32}-C_2H_4 complexes, the absorption spectra of the Au_{32} significantly change upon interaction with C_2H_4 in Orientation-1 and Orientation-3. The major peak of Au_{32} at 207 nm is shifted to 209 nm in Orientation-2. The major peaks of Orientation-1 and Orientation-3 are unclear from the computed data, but we observed nontrivial differences between the two spectra and consistent responses.

Based on these findings, we speculate that Au-based nanoclusters are more promising than Cu-based nanoclusters because of their coherent response of the UV-Vis spectra upon interaction with C_2H_4. In here, the spectral shifts and absorbance intensity variation owed to C_2H_4 adsorption on the metal clusters could be utilized for an optical sensor using portable UV-Vis spectrometers. Such optical sensors could be integrated into storage facilities to detect C_2H_4 concentrations. In addition, the aforementioned altered bandgap modifies the electronic conductivity of the Cu_{18} cluster, which could be measured via current-voltage (I-V) curves in a sensor device. This approach aligns with established methods for gas sensing using metal nanoparticles, where changes in electrical properties correlate with analyte adsorption.

The adsorption of C_2H_4 on the cellulose, chitosan, Cu_{18} cluster, and Au_{32} cluster is simulated using density functional theory. The calculations revealed that the adsorption of C_2H_4 on cellulose and chitosan is mainly driven by physisorption, as reflected by the low magnitude of adsorption energy and long-range interaction distances. Analyzing the ELF and frontier molecular orbitals verifies this claim. Meanwhile, Cu_{18} and Au_{32} interface with C_2H_4 revealed strong adsorption energy and orbital interactions, concluding that the interaction is driven by shared electron bonding or chemisorption. The electronic structure and optical spectra analysis

showed that Cu_{18} and Au_{32} are sensitive to C_2H_4, changing the bandgap and, thus, the UV-Vis absorption spectra intensity and peak position. Building from these findings, it is recommended to pursue work to study the electronic structure and I-V curve of the 2D materials decorated with metal clusters for C_2H_4 sensing performance. In addition, a study on the chemical functionalization of cellulose and chitosan can be beneficial for maximizing the potential of these biopolymers for trapping C_2H_4.

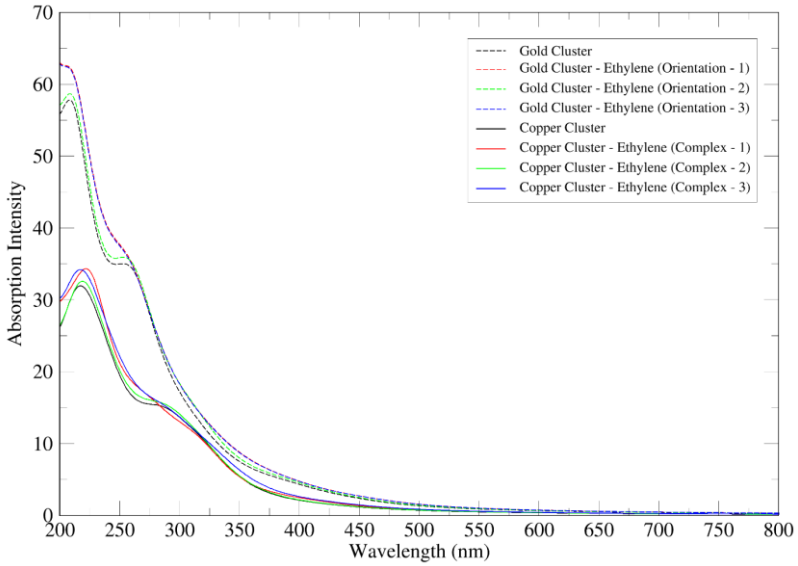

Figure 8. Absorbance spectra of Cu_{18}-C_2H_4 and Au_{18}-C_2H_4 complexes are indicated by solid lines and dashed lines, respectively. The spectrum is estimated using time-dependent density functional theory (TD-DFT) with 3,000 Lanczos iterations using the GGA-PBE exchange-correlation functional.

4. Conclusions

The mechanism of C_2H_4 adsorption on cellulose, chitosan, copper cluster (Cu_{18}), and gold cluster (Au_{32}) is studied using the framework of density functional theory. The results demonstrate that the interactions between cellulose-C_2H_4 and chitosan-C_2H_4 complexes are generally described as physisorption, where minor charge redistribution causes a weak attractive interaction. In addition, the magnitude of the adsorption energies of cellulose-C_2H_4 and chitosan-C_2H_4 is low (<0.5 eV), leading to a short recovery time value of less than a nanosecond. This claim is confirmed by the non-overlapping ELF at the interface and weak hybridization of frontier orbitals between constituents. Meanwhile, for Cu_{18}-C_2H_4 and Au_{32}-C_2H_4 systems, the adsorption is mainly characterized as chemisorption, where ELF basins and frontier orbitals of constituents overlap. This result leads to higher adsorption energy (>0.5) and a longer recovery time in seconds. The C_2H_4 adsorption on the Cu_{18} and Au_{32} resulted in a minor redistribution of electron density of states near the Fermi energy, changes in the bandgap of the clusters, and increases in the absorption intensity of the UV region.

This study evaluates the potential of biopolymers and metal clusters for C_2H_4 control technologies for postharvest agriculture. For future research on material synthesis, the findings suggest functionalizing biopolymers with metal nanoparticles such as Cu and Au nanoclusters to combine cellulose and chitosan's eco-friendly, scalable properties with the strong chemisorption of metal clusters, enhancing C_2H_4 trapping capabilities. Similarly, Cu and Au nanoclusters could be incorporated into chemiresistive sensors, utilizing bandgap changes for conductivity-based detection via current-voltage (I-V) measurements. Various derivatives and nanocomposites of cellulose and chitosan with nanomaterials are also worth exploring

experimentally and through simulation. The findings both provide directions in engineering materials for C_2H_4 control technologies and explain the fundamental adsorption mechanism of C_2H_4 on chitosan and cellulose biopolymers and Cu_{18} and Au_{32} metal clusters. This work provides a roadmap for tailoring low-cost biopolymers and high-efficiency metal clusters for agricultural storage systems. In addition, the findings presented here can also be extended to C_2H_4 adsorbents in the form of coatings and smart packaging systems.

Author Contributions

Conceptualization, A.A.Z.M. and C.B.M.; methodology, A.A.Z.M., C.B.M., A.A.G.P., R.M.R.H., and L.C.C.A.; software, A.A.Z.M., C.B.M., A.A.G.P., R.M.R.H. and L.C.C.A.; validation, L.C.C.A.; formal analysis, A.A.G.P. and R.M.R.H.; investigation, A.A.Z.M. and C.B.M.; resources, A.A.Z.M., C.B.M, A.A.G.P., R.M.R.H., and L.C.C.A.; data curation, R.M.R.H.; writing—original draft preparation, A.A.Z.M.; writing—review and editing, A.A.Z.M., C.B.M., A.A.G.P., R.M.R.H, and L.C.C.A.; visualization, A.A.G.P.; supervision, L.C.C.A.; project administration, A.A.Z.M.; All authors have read and agreed to the published version of the manuscript.

Institutional Review Board Statement

Not applicable.

Informed Consent Statement

Not applicable.

Data Availability Statement

Data supporting the findings of this study are available upon reasonable request from the corresponding author.

Funding

This research received support from the Western Mindanao State University through the project "*In Silico and Machine Learning-Assisted Materials Discovery for Ethylene Control Technologies in Postharvest Agriculture*".

Acknowledgments

A.A.Z.M. extends gratitude to the COARE supercomputing facility of the DOST-ASTI of the Philippine Government for providing the computational resources for the project. A.A.Z.M. acknowledges the auspicious support of the Physics Department, the College of Science and Mathematics, and the Office of Research Extension Services of the Western Mindanao State University.

Conflicts of Interest

The authors declare no conflict of interest.

References

1. Asrey, R.; Sharma, S.; Barman, K.; Prajapati, U.; Negi, N.; Meena, N.K. Biological and Postharvest Interventions to Manage the Ethylene in Fruit: A Review. *Sustainable Food Technol.* **2023**, *1*, 803–826, https://doi.org/10.1039/D3FB00037K.
2. Zhang, H.; Han, M.; Xie, Y.; Wang, M.; Cao, C. Application of Ethylene-Regulating Packaging in Postharvest Fruits and Vegetables Storage: A Review. *Packag. Technol. Sci.* **2022**, *35*, 461–471, https://doi.org/10.1002/pts.2644.
3. Jiang, Y.; Liu, Z.; Peydayesh, M.; Zhang, B.; Jia, X.; Huang, Q. Ethylene Control in Fruit Quality Assurance: A Material Science Perspective. *Aggregate* **2024**, *5*, e565, https://doi.org/10.1002/agt2.565.
4. Schudel, S.; Shoji, K.; Shrivastava, C.; Onwude, D.; Defraeye, T. Solution Roadmap to Reduce Food Loss along Your Postharvest Supply Chain from Farm to Retail. *Food Packag. Shelf Life* **2023**, *36*, 101057, https://doi.org/10.1016/j.fpsl.2023.101057.
5. Janssen, S.; Schmitt, K.; Blanke, M.; Bauersfeld, M.L.; Wöllenstein, J.; Lang, W. Ethylene Detection in Fruit Supply Chains. *Philos. Trans. R. Soc. A. Math. Phys. Eng. Sci.* **2014**, *372*, 20130311, https://doi.org/10.1098/rsta.2013.0311.
6. Hu, B.; Sun, D.-W.; Pu, H.; Wei, Q. Recent Advances in Detecting and Regulating Ethylene Concentrations for Shelf-Life Extension and Maturity Control of Fruit: A Review. *Trends Food Sci. Technol.* **2019**, *91*, 66–82, https://doi.org/10.1016/j.tifs.2019.06.010.
7. Alonso-Salinas, R.; López-Miranda, S.; Pérez-López, A.J.; Acosta-Motos, J.R. Strategies to Delay Ethylene-Mediated Ripening in Climacteric Fruits: Implications for Shelf Life Extension and Postharvest Quality. *Horticulturae* **2024**, *10*, 840, https://doi.org/10.3390/horticulturae10080840.
8. Tamošaitienė, J.; Parham, S.; Sarvari, H.; Chan, D.W.M.; Edwards, D.J. A Review of the Application of Synthetic and Natural Polymers as Construction and Building Materials for Achieving Sustainable Construction. *Buildings* **2024**, *14*, 2569, https://doi.org/10.3390/buildings14082569.
9. Ally, N.; Gumbi, B. A review on metal nanoparticles as nano-sensors for environmental detection of emerging contaminants. *Mater. Today Proc.* **2023**, https://doi.org/10.1016/j.matpr.2023.08.032.
10. Dewangan, K.; Kant, T.; Shrivas, K. Chapter 30 - Copper nanoparticle-based sensors for environmental pollutions. In Copper Nanostructures: Next-Generation of Agrochemicals for Sustainable Agroecosystems, Abd-Elsalam, K.A., Ed.; Elsevier: **2022**; pp. 751-774, https://doi.org/10.1016/B978-0-12-823833-2.00001-5.
11. Zeng, S.; Yong, K.-T.; Roy, I.; Dinh, X.Q.; Yu, X.; Luan, F. A Review on Functionalized Gold Nanoparticles for Biosensing Applications. *Plasmonics* **2011**, *6*, 491–506, https://doi.org/10.1007/s11468-011-9228-1.
12. Dehghani, M.H.; Ahmadi, S.; Ghosh, S.; Othmani, A.; Osagie, C.; Meskini, M.; AlKafaas, S.S.; Malloum, A.; Khanday, W.A.; Jacob, A.O.; et al. Recent Advances on Sustainable Adsorbents for the Remediation of Noxious Pollutants from Water and Wastewater: A Critical Review. *Arab. J. Chem.* **2023**, *16*, 105303, https://doi.org/10.1016/j.arabjc.2023.105303.
13. Bakhtiari, S.; Salari, M.; Shahrashoub, M.; Zeidabadinejad, A.; Sharma, G.; Sillanpää, M. A Comprehensive Review on Green and Eco-Friendly Nano-Adsorbents for the Removal of Heavy Metal Ions: Synthesis, Adsorption Mechanisms, and Applications. *Curr. Pollut. Rep.* **2024**, *10*, 1–39, https://doi.org/10.1007/s40726-023-00290-7.
14. Rana, A.K.; Mostafavi, E.; Alsanie, W.F.; Siwal, S.S.; Thakur, V.K. Cellulose-Based Materials for Air Purification: A Review. *Ind. Crop. Prod.* **2023**, *194*, 116331, https://doi.org/10.1016/j.indcrop.2023.116331.
15. Fathalian, F.; Moghadamzadeh, H.; Hemmati, A.; Ghaemi, A. Efficient CO2 Adsorption Using Chitosan, Graphene Oxide, and Zinc Oxide Composite. *Sci. Rep.* **2024**, *14*, 3186, https://doi.org/10.1038/s41598-024-53577-0.
16. Liu, D.; Wang, Z.; Jiang, X. Gold Nanoparticles for the Colorimetric and Fluorescent Detection of Ions and Small Organic Molecules. *Nanoscale* **2011**, *3*, 1421–1433, https://doi.org/10.1039/C0NR00887G.
17. Ramadass, K.; Lakhi, K.S.; Sathish, C.I.; Ruban, A.M.; Bahadur, R.; Singh, G.; Gujral, H.S.; Al-Abri, M.; Al-Muhtaseb, A.a.H.; Tavakkoli, E.; Yi, J.; Karakoti, A.; Vinu, A. Copper nanoparticles decorated N-doped mesoporous carbon with bimodal pores for selective gas separation and energy storage applications. *Chem. Eng. J.* **2022**, *431*, 134056, https://doi.org/10.1016/j.cej.2021.134056.
18. Moghaddam-Manesh, M.; Darvishi, R.; Moshkriz, A. Innovative High-Performance Antimicrobial Agent and Dye Adsorbent Based on Magnetic/Copper Nanoparticles. *J. Polym. Environ.* **2024**, *32*, 5231–5253, https://doi.org/10.1007/s10924-024-03289-3.

19. Chen, D.; Zhou, W.; Ji, Y.; Dong, C. Applications of Density Functional Theory to Corrosion and Corrosion Prevention of Metals: A Review. *Mater. Genome Eng. Adv.* **2025**, *3*, e83, https://doi.org/10.1002/mgea.83.
20. Liao, X.; Lu, R.; Xia, L.; Liu, Q.; Wang, H.; Zhao, K.; Wang, Z.; Zhao, Y. Density Functional Theory for Electrocatalysis. *Energy Environ. Mater.* **2022**, *5*, 157–185, https://doi.org/10.1002/eem2.12204.
21. van Mourik, T.; Bühl, M.; Gaigeot, M.-P. Density Functional Theory across Chemistry, Physics and Biology. *Philos. Trans. A Math. Phys. Eng. Sci.* **2014**, *372*, 20120488, https://doi.org/10.1098/rsta.2012.0488.
22. Jelil, J.; Abdurahman, A.; Gülseren, O.; Schwingenschlogl, U. Non-Covalent Functionalization of Single Wall Carbon Nanotubes and Graphene by a Conjugated Polymer. *Appl. Phys. Lett.* **2014**, *105*, 013103–013103, https://doi.org/10.1063/1.4886968.
23. Barker, D.; Fors, A.; Lindgren, E.; Olesund, A.; Schröder, E. Filter Function of Graphene Oxide: Trapping Perfluorinated Molecules. *J. Chem. Phys.* **2020**, *152*, 024704, https://doi.org/10.1063/1.5132751.
24. Mazumder, J.T.; Jha, R.K. Theoretical Insights into Gas Sensing Properties of MXene. *Sens. Actuators Rep.* **2023**, *6*, 100174, https://doi.org/10.1016/j.snr.2023.100174.
25. Weng, K.; Peng, J.; Shi, Z.; Arramel, A.; Li, N. Highly NH3 Sensitive and Selective Ti3C2O2-Based Gas Sensors: A Density Functional Theory-NEGF Study. *ACS Omega* **2023**, *8*, 4261–4269, https://doi.org/10.1021/acsomega.2c07492.
26. Khakbaz, P.; Moshayedi, M.; Hajian, S.; Soleimani, M.; Narakathu, B.; Bazuin, B.J.; Pourfath, M.; Atashbar, M. Titanium Carbide MXene as NH 3 Sensor: Realistic First-Principles Study. *J. Phys. Chem. C* **2019**, *123*, 29794–29803, https://doi.org/10.1021/acs.jpcc.9b09823.
27. Shukri, G.; Kasai, H. Density Functional Theory Study of Ethylene Adsorption on Clean Anatase TiO2 (001) Surface. *Surface Sci.* **2014**, *619*, 59–66, https://doi.org/10.1016/j.susc.2013.09.022.
28. Aydın, F.; Sel, K. Adsorption of Ethylene and 1-Methylcyclopropene (1-MCP) on Al-Doped Graphene Structure: A DFT Study for Gas Sensing Application. *J. Turk. Chem. Soc. A: Chem.* **2024**, *11*, 1535–1544, https://doi.org/10.18596/jotcsa.1492945.
29. Tabari, L.; Farmanzadeh, D. Yttrium Doped Graphene Oxide as a New Adsorbent for H2O, CO, and Ethylene Molecules: Dispersion-Corrected DFT Calculations. *Appl. Surf. Sci.* **2020**, *500*, 144029, https://doi.org/10.1016/j.apsusc.2019.144029.
30. Rad, A.S.; Ayub, K. Adsorption Properties of Acetylene and Ethylene Molecules onto Pristine and Nickel-Decorated Al12N12 Nanoclusters. *Mater. Chem. Phys.* **2017**, *194*, 337–344, d https://doi.org/10.1016/j.matchemphys.2017.04.002.
31. Li, X.; Xu, C.; Du, X.; Wang, Z.; Huang, W.; Sun, J.; Wang, Y.; Li, Z. Assembled Reduced Graphene Oxide/Tungsten Diselenide/Pd Heterojunction with Matching Energy Bands for Quick Banana Ripeness Detection. *Foods* **2022**, *11*, 1879, https://doi.org/10.3390/foods11131879.
32. Giannozzi, P.; Baroni, S.; Bonini, N.; Calandra, M.; Car, R.; Cavazzoni, C.; Ceresoli, D.; Chiarotti, G.L.; Cococcioni, M.; Dabo, I.; et al. QUANTUM ESPRESSO: A Modular and Open-Source Software Project for Quantum Simulations of Materials. *J. Phys.: Condens. Matter.* **2009**, *21*, 395502, https://doi.org/10.1088/0953-8984/21/39/395502.
33. Giannozzi, P.; Baseggio, O.; Bonfà, P.; Brunato, D.; Car, R.; Carnimeo, I.; Cavazzoni, C.; de Gironcoli, S.; Delugas, P.; Ferrari Ruffino, F.; Ferretti, A.; Marzari, N.; Timrov, I.; Urru, A.; Baroni, S. Quantum ESPRESSO toward the Exascale. *J. Chem. Phys.* **2020**, *152*, 154105, https://doi.org/10.1063/5.0005082.
34. Hamann, D.R. Optimized Norm-Conserving Vanderbilt Pseudopotentials. *Phys. Rev. B* **2013**, *88*, 085117, https://doi.org/10.1103/PhysRevB.88.085117.
35. Perdew, J.P.; Burke, K.; Ernzerhof, M. Generalized Gradient Approximation Made Simple. *Phys. Rev. Lett.* **1996**, *77*, 3865–3868, https://doi.org/10.1103/PhysRevLett.77.3865.
36. Grimme, S.; Antony, J.; Ehrlich, S.; Krieg, H. A Consistent and Accurate Ab Initio Parametrization of Density Functional Dispersion Correction (DFT-D) for the 94 Elements H-Pu. *J. Chem. Phys.* **2010**, *132*, 154104, https://doi.org/10.1063/1.3382344.
37. Koumpouras, K.; Larsson, J.A. Distinguishing between Chemical Bonding and Physical Binding Using Electron Localization Function (ELF). *J. Phys.: Condens. Matter.* **2020**, *32*, 315502, https://doi.org/10.1088/1361-648X/ab7fd8.
38. Momma, K.; Izumi, F. VESTA: A Three-Dimensional Visualization System for Electronic and Structural Analysis. *J. Appl. Cryst.* **2008**, *41*, 653–658, https://doi.org/10.1107/S0021889808012016.
39. Momma, K.; Izumi, F. VESTA 3 for Three-Dimensional Visualization of Crystal, Volumetric and Morphology Data. *J. Appl. Cryst.* **2011**, *44*, 1272–1276, https://doi.org/10.1107/S0021889811038970.

40. Malcıoğlu, O.B.; Gebauer, R.; Rocca, D.; Baroni, S. turboTDDFT – A Code for the Simulation of Molecular Spectra Using the Liouville–Lanczos Approach to Time-Dependent Density-Functional Perturbation Theory. *Comput. Phys. Commun.* **2011**, *182*, 1744–1754, https://doi.org/10.1016/j.cpc.2011.04.020.
41. Ge, X.; Binnie, S.J.; Rocca, D.; Gebauer, R.; Baroni, S. turboTDDFT 2.0—Hybrid Functionals and New Algorithms within Time-Dependent Density-Functional Perturbation Theory. *Comput. Phys. Commun.* **2014**, *185*, 2080–2089, https://doi.org/10.1016/j.cpc.2014.03.005.
42. Dri, F.L.; Shang, S.; Hector, L.G.; Saxe, P.; Liu, Z.-K.; Moon, R.J.; Zavattieri, P.D. Anisotropy and Temperature Dependence of Structural, Thermodynamic, and Elastic Properties of Crystalline Cellulose Iβ: A First-Principles Investigation. *Modelling Simul. Mater. Sci. Eng.* **2014**, *22*, 085012, https://doi.org/10.1088/0965-0393/22/8/085012.
43. Yui, T.; Uto, T.; Ogawa, K. Molecular and Crystal Structure of a Chitosan?Zinc Chloride Complex. *Nanomaterials* **2021**, *11*, 1407, https://doi.org/10.3390/nano11061407.
44. Simão, C.D.; Reparaz, J.S.; Wagner, M.R.; Graczykowski, B.; Kreuzer, M.; Ruiz-Blanco, Y.B.; García, Y.; Malho, J.-M.; Goñi, A.R.; Ahopelto, J.; et al. Optical and Mechanical Properties of Nanofibrillated Cellulose: Toward a Robust Platform for next-Generation Green Technologies. *Carbohydr. Polym.* **2015**, *126*, 40–46, https://doi.org/10.1016/j.carbpol.2015.03.032.
45. Fauzi, N.I.M.; Fen, Y.W.; Omar, N.A.S.; Saleviter, S.; Daniyal, W.M.E.M.M.; Hashim, H.S.; Nasrullah, M. Nanostructured Chitosan/Maghemite Composites Thin Film for Potential Optical Detection of Mercury Ion by Surface Plasmon Resonance Investigation. *Polymers* **2020**, *12*, 1497, https://doi.org/10.3390/polym12071497.
46. Rad, A.S.; Aghaei, S.M.; Poralijan, V.; Peyravi, M.; Mirzaei, M. Application of Pristine and Ni-Decorated B12P12 Nanoclusters as Superior Media for Acetylene and Ethylene Adsorption: DFT Calculations. *Comput. Theor. Chem.* **2017**, *1109*, 1–9, https://doi.org/10.1016/j.comptc.2017.03.030.
47. do Nascimento Sousa, S.D.; Santiago, R.G.; Soares Maia, D.A.; de Oliveira Silva, E.; Vieira, R.S.; Bastos-Neto, M. Ethylene Adsorption on Chitosan/Zeolite Composite Films for Packaging Applications. *Food Packag. Shelf Life* **2020**, *26*, 100584, https://doi.org/10.1016/j.fpsl.2020.100584.
48. Bernardo, C.G.P.M.; Gomes, J.A.N.F. The Adsorption of Ethylene on the (110) Surfaces of Copper, Silver and Platinum: A DFT Study. *J. Mol. Struct.* **2002**, *582*, 159–169, https://doi.org/10.1016/S0166-1280(01)00771-0.
49. Kang, G.-J.; Chen, Z.-X.; Li, Z. Theoretical Studies of the Interactions of Ethylene and Formaldehyde with Gold Clusters. *J. Chem. Phys.* **2009**, *131*, 034710, https://doi.org/10.1063/1.3167408.
50. Shtepliuk, I.; Caffrey, N.M.; Iakimov, T.; Khranovskyy, V.; Abrikosov, I.A.; Yakimova, R. On the Interaction of Toxic Heavy Metals (Cd, Hg, Pb) with Graphene Quantum Dots and Infinite Graphene. *Sci. Rep.* **2017**, *7*, 3934, https://doi.org/10.1038/s41598-017-04339-8.

Publisher's Note & Disclaimer